EXPANDING TECHNICAL AND TECHNOLOGICAL POSIBILITIES IN THE PRODUCTION OF PARTS AND TOOLS USING BRONZES

TETIANA KIMSTACH[1], ANTON PANDA[2,6], KOSTIANTYN DYADYURA[3,4], KOSTIANTYN UZLOV[1], LIUDMYLA SOLONENKO[3], SERGEY REPYAKH[5]

[1]Faculty of Quality and Material Engineering, Ukrainian State University of Science and Technology, Dnipro, Ukraine

[2]Faculty of Manufacturing Technologies with a seat in Presov, Technical University of Kosice, Presov, Slovak Republic

[3]Department of Biomedical Engineering, Odesa Polytechnic National University, Odesa, Ukraine

[4]Department of Agricultural Engineering, Odesa State Agrarian University, Odesa, Ukraine

[5]Faculty of Electomechanics and Electrometallurgy, Ukrainian State University of Science and Technology, Dnipro, Ukraine

[6]Institute of Technology and Business in Ceske Budejovice, Faculty of Technology, Department of Mechanical Engineering, Ceske Budejovice, Czech Republic

DOI: 10.17973/MMSJ.2026_06_2026113

anton.panda@tuke.sk

Among the known standardized bronze grades, there are currently no foundry structural bronzes that would simultaneously combine both non-magnetism and corrosion resistance, in particular, in tap water and seawater. The presence of bronze with such a list of preferential properties will allow not only to expand the boundaries of bronzes as a structural material using, but also to provide prospects for increasing and expanding the technical and technological capabilities of new equipment and technologies in the field of shipbuilding, aircraft construction, instrument making, etc. Today, the only bronze with such a list of properties is aluminum bronze BrA7K2O1.5Mts2, in which, nevertheless, corrosion resistance in comparison with known standardized bronze grades has not yet been studied. All bronzes studied in this work, except for bronze BrO6C6C3, are absolutely stable in warm standing tap water with a cyclic change in temperature from 30 to 50 °C. With the exception of BrA9Zh3L bronze brand, all other bronzes studied in the work are stable in warm standing artificial seawater with a daily change in temperature from 30 to 50 °C and on a ten-point scale have the 4th point of corrosion resistance. The greatest corrosion resistance is possessed by bronze BrA7K2O1.5Mts0.3 with a value of K_R = 0.47…0.63. Corrosion in samples of BrA7K2O1.5Mts0.3 bronze, which are after their heat treatment and without heat treatment, is equally continuous. Bronze BrA7K2O1.5Mts0.3 without heat treatment in cold standing artificial seawater is more corrosion-resistant if it is cast in a chill mold. At the same time, in all corrosive environments used in the work, the corrosion resistance of bronze BrA7K2O1.5Mts0.3 is more affected by its heat treatment than by in its chemical composition changing. Further development was received by ideas about the corrosion resistance of non-magnetic structural cast aluminum bronzes in tap water and artificial seawater, taking into account the initial state of the bronzes and the corrosive environment condition. For the first time, in comparison with standardized corrosion-resistant bronze grades, data were obtained on the corrosion rate of “as-cast” and heat-treated non-magnetic bronze BrA7K2O1.5Mts0.3 in warm tap water, warm and cold artificial sea water. This will allow making a well-founded choice of bronzes for the operation of products made of them in the environments and conditions used in this work or close to them. This will save time, financial costs and material resources for developers of new machines, assemblies and units to make a rational or optimal technical decision regarding a rational product material.

KEYWORDS

non-magnetic bronze, corrosion, water, aluminum, nickel, structure, temperature, heat treatment

1 INTRODUCTION

Foundry bronzes are used to manufacture parts used in mechanical, shipbuilding, aircraft, machine-tool, instrument-making and other industries. In particular, among the varieties of industrial valves, there is a shut-off valve, which is made of aluminum bronze and is widely used in the chemical, oil and gas, pulp and paper industries, mining and energy industries, as part of river and marine floating facilities, as well as port infrastructure, in desalination and water purification systems. According to the results of analytical research by Precedence Research (2024), if the global market for industrial valves made of various alloys in 2024 was 76.90 billion US dollars, then, according to forecasts, from 2025 to 2034, it will increase from 86.67 to 250.84 billion US dollars. Foundry bronzes are used to manufacture parts whose material must be strong, maintainable, reliable and resistant to corrosion and wear, which, in some cases, allows the use of bronze parts instead of steel. In addition to the above characteristics, depending on the operating conditions of cast parts, additional requirements may be imposed on bronzes, in particular:

– resistance to biofouling and biocorrosion, which is, for example, necessary for ships and port facilities;

– cavitation resistance, which is, for example, important for pumps and ship propellers;

– plasticity at low temperatures, which is, for example, important for cryogenics, aircraft, and ships operating in “high” northern or southern latitudes;

– absence of magnetism (non-magnetism), which is, for example, important for engines of mine hunters, submarines, some types of medical equipment, compasses, telescopes, measuring instruments;

– absence of sparks, which is, for example, important for metalworking tools used on offshore platforms, oil refineries, in gas pumping networks and stations, etc. [Nadolski 2017].

Among the foundry bronzes that are most in demand in industry are non-magnetic alloys of the Cu-Sn system (tin bronzes). Tin bronzes have relatively high corrosion resistance, antifriction properties, good machinability, and do not give sparks when struck. Two-component bronzes are used for musical instruments and bells [Aliyu 2025] manufacturing. A significant disadvantage of tin bronzes is their relatively low level of mechanical properties, as well as a large temperature range of crystallization, which negatively affects their casting properties and the tightness of cast products made from them.

Non-magnetic and slightly magnetic, corrosion-resistant bronzes also include aluminum bronzes, which are divided into four conventional types according to their chemical and phase composition.

The first type is single-phase non-magnetic two-component (Cu-Al) low-alloy bronzes (α-alloys), which contain up to 8% Al by mass. Under certain conditions, a hard but brittle γ_2-phase may

appear in the structure of such bronzes, which, according to [Song 2015 & 2022], is undesirable, since the high Al content in the γ_2-phase contributes to level of corrosion resistance of bronzes decreasing. Bronzes of this type have relatively low tensile strength but high ductility. In this regard, they are mainly used for the manufacture of products by plastic deformation.

The second type is two-phase (duplex) high-alloying alloys with a mass content of Al = 8...12% and, as a rule, with the addition of nickel and iron, which give them a certain level of strength but, like ferromagnetic metals, also magnetism. The presence of a two-phase structure in the cast state makes it possible to increase the mechanical properties of such bronzes, both in the "as-cast" and in the heat-treated state, to manufacture products from them both by casting and deformation [Turtelli 2006]. However, aluminum-iron-nickel bronzes are characterized by low casting properties, uneven structure in the as-cast state, and a tendency to develop shrinkage porosity in castings, which can cause a decrease in the corrosion resistance of cast parts [Wu 2015, Gaspar 2018, Ocejo 2022, Li 2022, Qiao 2019].

The third type is single-phase three-component aluminum-silicon bronzes (α-alloys), which, while maintaining a high level of plasticity, achieve high strength due to their plastic deformation. Today, the only such standardized in industrialized countries of the world is bronze with a mass content of silicon ~2% and aluminum ~7% ($CuAl_7Si_2$). $CuAl_7Si_2$ bronze is slightly magnetic, but stronger than the bronzes of the first group. Products are mainly made from such bronzes by plastic deformation and/or mechanical processing (parts of automobile engines, equipment for pole-mounted electric lines, fasteners, valve components, cams, hardware for marine use, etc.) and, to a limited extent, by casting [Kuric 2022].

The fourth type is magnetic multiphase highly alloyed aluminum-manganese bronzes with a mass content of Mn ~13%, Al = 8...9%. Such bronzes are characterized by high casting properties and are mainly used for the manufacture of propellers for ships and boats. Multiphase aluminum-manganese bronzes are less durable than bronzes of the second type, but have good weldability, resistance to erosion and cavitation. Magnetic properties are given to these bronzes by intermetallics consisting of Cu, Al and Mn. To reduce magnetism, cast products made of this bronze are heat-treated. It should be noted that this type also includes low-magnetic bronze BrA9Mts2L with a content of Al=8…9.5% Mn=1.5…2.5%, $\boldsymbol{Fe} \leq \mathbf{1}\%$ and $\boldsymbol{Zn} \leq \mathbf{1.5}\%$, which has the inherent disadvantages of aluminum-manganese bronzes with a higher Mn content, and the magnetism of such bronzes is given by the Fe impurity.

Thus, despite the significant number of existing bronzes, there are currently no foundry structural bronzes that would simultaneously combine high strength, non-magnetism, and corrosion resistance in natural environments [Coranic 2023]. Bronzes with such a list of preferential properties will not only expand the scope of bronze use as a structural material but will also provide prospects for improving and expanding the technical and technological capabilities of new equipment and technologies.

Purpose of this work is to investigate the influence of the chemical composition of bronze $BrA_7K_2O1.5Mts0.3$, the conditions of solidification in the casting mold and heat treatment on its corrosion resistance in standing tap water and artificial seawater in comparison with standardized bronze grades.

2 STATUS OF THE ISSUE

Currently, among the bronzes resistant to corrosion, in particular, in seawater, the most widely used industrially are magnetic aluminum-nickel bronzes (NAB) - bronzes of the second type. NAB bronzes are aluminum bronzes with Al = 9...12%, which are additionally alloyed with 4...6% Ni and Fe and may contain Mn. In NAB, only Ni and Al increase their corrosion resistance, forming a continuous protective film of oxidation products on the surface of bronze products. At the same time, over time, the rate of oxidation of NAB in seawater slows down until the protective film reaches a long-term steady state. According to [Siemek 2021] and [Mayer 2022] with co-authors, the slowdown in the corrosion rate of aluminum bronze products in seawater is due to the formation of a continuous passive film of oxides. According to [Qin 2022, Zeng 2022] such a protective film can consist of two layers, where the outer layer is copper oxide, the inner one is aluminum oxide. According to [Li 2019, Song 2022, Luo 2018, Zhang 2019, Tian 2022], such a protective film is formed from the moment of contact of an aqueous NaCl solution with the bronze surface as a result of the sequential passage of the following chemical reactions:

$$Cu + 2Cl^- \rightarrow CuCl_2^- + e^-, \quad (1)$$

$$2CuCl_2^- + H_2O \rightarrow Cu_2O + 4Cl^- + 2H^+, \quad (2)$$

$$2Cu_2O + O_2 \rightarrow 4CuO, \quad (3)$$

$$Al + 4Cl^- \rightarrow AlCl_4^- + 3e^-, \quad (4)$$

$$AlCl_4^- + 2H_2O \rightarrow Al_2O_3 + 3H^+ + 4Cl^-. \quad (5)$$

At the same time, according to [Song 2023], the Al_2O_3 layer formed on the surfaces of products with NAB by reactions (1)…(5) is so strong that it provides them with not only high corrosion, but also erosion cavitation resistance. As noted above, the corrosion resistance of NAB largely depends on its microstructure. According to [Asgari 2021] with colleagues and authors of the work [Wu 2015], the structure of cast NAB is multiphase and consists of a copper α-phase, a residual martensitic β-phase and four intermetallic kappa phases (κ_I...κ_{IV}), which can negatively affect the corrosion resistance of NAB. In addition, one of the reasons that reduce the corrosion resistance of NAB in the marine environment is the size of its structural components. As noted by [Asgari 2021, Cargua 2021], with slow cooling of castings in the mold (0.01...0.10 °C/s), the size of its microstructural components increases. As a result, according to [Vinagre 2020, Kimstach 2025a], with an increasing in the size of microstructural components, the level of both mechanical properties and operational properties of cast NABs decreases.

The refinement of the microstructural components of NAB is usually achieved by carrying out their appropriate heat treatment. For example, to increase the corrosion resistance of NAB products, according to the British Navy standard NES747. Part 2: Heat treatment is performed in such a way as to minimize or eliminate the β-phase from the NAB microstructure and increase the density of κ-phase precipitates in the α-phase. According to [Ocejo 2022, Kimstach 2025b], the use of different critical temperatures and cooling rates allows to obtain NAB with a microstructure that can be Widmanstatten-α, bainitic or martensitic-β, which significantly changes not only the level of mechanical, but also corrosion properties of the alloys.

The paper [Siemek 2021, Panda 2011a] presents the results of research on the corrosion process of heat-treated aluminum-nickel (NAB - CuAl10Fe5Ni5) and aluminum-manganese (MAB - CuMn12Al8Fe4Ni2) bronze in solutions that imitate sea (SSW) and fresh (SFW) water, which were prepared according to the DIN 50905-4 standard, section 4.1 and supplemented with chemical reagents $FeCl_3$ and NH_4OH. It was established that the main negative effect of heat treatment on the corrosion of cast NAB and MAB samples is determined by the amount and nature

of the distribution of the β-phase in the alloy structure, which is prone to selective corrosion in both electrolytes.

From the analysis of the results of the studies by [Nadolski 2017, Song 2022, Valicek 2016, Jurko 2011, Panda 2013a], it follows that the same phase can play different roles in the selective corrosion of NAB under different environmental conditions. In particular, [Jurko 2012] found that changing the pH value (pH) has different effects on the selective phase corrosion of NAB in a 3.5% NaCl solution. That is, in a 3.5% NaCl solution with a pH value of < 4, κ-phases are mainly dissolved in the NAB structure, while at pH > 4, the α-phase is mainly dissolved in bronze.

In [Siemek 2021, Zhang 2019, Jurko 2013], the authors note that heat treatment of NAB reduces their resistance to corrosion in salt water, and the multiphase microstructure of NAB is prone to selective phase corrosion due to the difference in the chemical composition and crystal structure of the phases, which leads to the occurrence of galvanic type of corrosion. At the same time, the corrosion behavior of NAB varies depending on the pH level of the solution, as well as the type and amount of aggressive ions in it, which is confirmed by the data of [Zhang 2019, Tian 2022, Panda 2011b & 2013b].

According to [Dyadyura 2017a, Qiao 2019, Nahornyi 2022, Mascenik 2024] and other authors, in addition to heat treatment, there are other methods of structural components lessening in the surface layer of NAB products, for example, by friction with mixing, shot blasting or laser melting of the surface layers of products, etc. [Krenicky 2024]. Unlike heat treatment, these methods of grain sizes lowering and homogenization of the microstructure can be applied only in individual cases or in individual areas of bronze products, which, in particular, was noted in the works of [Harnicarova 2019, Zaloga 2019, Vinagre 2020, Cargua 2021], and is due to the limited technological capabilities of implementing certain methods, the design of the product or the conditions of its use. The corrosion resistance of bronzes varies in different environments [Qiao 2019, Zaloga 2020] and depends on a significant number of factors, including their condition (cast, deformed, heat treated, etc.). This is evidenced, in particular, by the experimental data of [Qin 2022, Dyadyura 2017b] on the corrosion rate (W) of copper and its alloys in drinking water in New York City (United States of America), which are given in Table 1, the data of [Siemek 2021]) in Table 2 and the data of [Mayer 2022] in Table 3.

Table 1. Corrosion rates of copper and its alloys in drinking water in New York City

Metal, alloy	Chemical composition, % (by weight)								W, mm/year
	Cu	Al	Fe	Ni	Mn	Zn	Sn	Pb	
Deformed copper	99.9								0.017
Cast Ni-Cu alloy	31		1.4	66	0.9				0.040
Cast Cu-Ni alloy	88		1	10	0.4				0.011
Cast aluminum bronzes	80	11	4	5					0.003*; 0.005*
	85	11	4						0.202
	88	9	2						0.003*; 0.008*
	90	9	1						0.105
Cast tin bronzes	88					1	11		0.005
	88					3	8		0.008
Deformed tin bronze with 0.2% R	92						8		0.011
Cast valve bronze	88					4	6	1.6	0.005
Cast nickel-tin bronze	89			5			5		0.025

Notes. * – cast bronze products from various manufacturers

Using extracts from British Standards (Aluminum Bronze Alloys for Industry [Kimstach 2025a]) and manuals (Manuals on Engineering Alloys Used in the British Naval Service 01/2: Technical Data Sheets.), for wrought and cast bronze products, [Aliyu 2025] provides data on their corrosion rates in flowing seawater and cavitation erosion rates in tap water, which are given in Table 2.

Table 2. Corrosion rate of bronzes in flowing seawater and cavitation erosion rate of bronzes in tap water

Bronze, alloy	W in flowing seawater, mm/year		Cavitation erosion rate in tap water, mm^3/h
	general	slit	
Deformed alloys			
Cu-Ni 90/10	0.040	< 0.040	
Cu-Ni 70/30	0.025	< 0.025	
Bronze with 5% Al	0.060	< 0.060	
Bronze with 8% Al	0.050	< 0.050	
Bronze with 9% Al	0.060	0.075	
Nickel-aluminum bronze (NAB)	0.075	< 0.500	
Aluminum-silicon bronze	0.060	< 0.074	
Foundry alloys			
Aluminum bronze	0.060	< 0.06	0.8
Nickel-aluminum bronze (NAB)	0.060	< 0.06	0.6
Aluminum-manganese bronze	0.040	3.8	1.5
Monel alloy with 3-4% Si	0.025	0.5	1.2-2.8

Notes. To determine the total corrosion rate and crevice corrosion, the samples were completely immersed in seawater for 1 year under rafts in Langstone Harbour. The crevice corrosion rate was assessed on samples that were fixed in Plexiglas clamps. To determine erosion resistance, the samples were exposed to an underwater water-air jet at a temperature of 60 °C, which emerged onto each sample from a 0.4 mm diameter pipe located 1...2 mm from the sample.

According to [Cargua2021], the corrosion rate in seawater (W) of different metals and alloys varies widely, as evidenced by the data in Table. 3.

Table 3. Corrosion rate in seawater (W) of various metals and alloys

Metal	W, mm/year	Alloy	W, mm/year	Alloy	W, mm/year
Ti	0.001	Phosphor bronze with 3% or 10% Sn	0.020	Silicon bronze	0.035
Sn	0.030	Aluminum bronze with 10% Al	0.020	Marine brass	0.040
Cu	0.030	Aluminum-silicon bronze	0.015	Aluminum brass	0.010
Zn	0.050	Nickel-aluminum bronze (NAB)	0.015	Mild steel	0.130

A large number of works are devoted to the issue of corrosion resistance of aluminum bronzes. In particular, in work [Mayer 2022] the corrosion rate of aluminum bronzes (CuAl4.5; CuAl7.1 and CuAl10.1) in artificial seawater (ASTM D1141) with pH=10±0.3 was determined. At the same time, data on the corrosion rate were compared with the content of Al and Sn in these bronzes. It was established that the higher the aluminum content in the bronze, the lower the corrosion rate, for the maximum limit of the content in the bronze Al = 10.11% and Sn = 0.13%.

A particular problem for the corrosion resistance of metal products is biofouling - a process that occurs in seawater and is accompanied not only by the settlement of macrofouling organisms (ascidians, hydroids, sponges, sea acorns) on metal

products, but also leads to a sharp increase in the corrosion rate, costs and reduced service life of underwater constructions, etc. [Kimstach 2025b, Panda 2011b].

Biofouling and, accordingly, the corrosion rate depend on a significant number of factors, including the geographical location of the sea. The authors of [Kimstach 2025a] found that, being in natural seawater for 18 months, the corrosion rate of NAB samples in the first months of testing reached 1.27 mm/year, after which it decreased to 0.11 mm/year, which, however, is significantly higher than the corrosion rate in artificial seawater (0.06 mm/year) and in air. Based on this, to predict the service life of metal products, the authors of [Kimstach 2025b] recommend conducting corrosion tests in natural seawater, i.e. taking into account the influence of changes in its temperature, speed of movement, salinity, illumination, concentration of nitrates and sulfates dissolved in it, oxygen, etc.

From the above it follows that:

- today non-magnetic structural cast aluminum bronze, resistant to corrosion in tap water and sea water, is generally unknown;
- the corrosion rate of any bronze depends on a significant number of factors, including its chemical and phase composition, product operating conditions, chemical and biological composition of the corrosive environment, the value of the hydrogen index of the environment, etc.
- the development or selection of any alloy, or the development of the heat treatment regime of the alloy for the operation of any product in specific conditions and environment should be targeted;
- from the point of view of corrosion resistance, the selection of the appropriate chemical composition of bronze, the conditions of its solidification in the casting mold should be carried out only according to the results of a comparative assessment of the relative corrosion resistance from a number of standardized alloys selected for this purpose;
- information on the influence of the chemical composition of bronze BrA7K2O1.5Mts0.3, the conditions of solidification in the casting mold and heat treatment on its corrosion resistance, in particular, in tap water and artificial seawater, is currently lacking.

3 MATERIALS AND METHODS

The non-contact corrosion resistance of bronzes was assessed using a ten-point scale given in [Valicek 20]. To assess the synergistic effect of the chemical composition of BrA78K2O10.5Mts0.3 bronze on its corrosion resistance, the K_R criterion was used, which was calculated using the equation [Qiao 2019, Panda 2013b]:

$$K_R = (1–0{,}01 \cdot nn) \cdot (Al\text{-}Si\text{-}Mn)/(1+Sn)^2 \quad (6)$$

where Al, Si, Mn, Sn, nn – mass content of aluminum, silicon, manganese, tin and undesirable impurities in bronze, respectively, % Non-contact corrosion resistance in warm standing tap water and artificial sea water was carried out on samples in the form of washers ∅40×10 mm of not heat-treated ("as-cast") bronzes BrA10Zh4N4L, BrA9Zh3L, BrO6Ts6S3, BrA7K2O1.5Mts0.3L (K_R=0.34), BrA7K2O1.5Mts0.3L (K_R=0.57), BrA7K2O1.5Mts0.3L (K_R=0.77) and heat-treated bronzes BrA7K2O1.5Mts0.3L (K_R=0.34), BrA7K2O1.5Mts0.3L (K_R=0.57), BrA7K2O1.5Mts0.3L (K_R=0.77).

The samples were cut from ingots ∅50×190 mm, which were cast in sand-sodium-silicate molds, and their surface roughness was assured to the purity of Rz20, which was measured on a profilometer mod. 296. The use of such samples was aimed at determining the influence of liquation processes that may accompany the solidification of the melt in the mold, on the nature of their corrosion and stability in an environment with acidic properties. In addition to the "as-cast" samples from bronze BrA7K2O1.5Mts0.3, samples were studied thermally treated according to the following regime: heating the samples to 770 °C and isothermal holding for 30…35 min, quenching from 770 °C in water with a temperature of 20 °C and ageing at 300 °C for 1 hour.

Corrosion in tap water and seawater is an electrochemical process, the speed and nature of which, as noted above, depend on a huge number of factors. Based on this, the determination of the overall corrosion resistance of bronzes was carried out according to an accelerated test scheme in standing warm tap water (drinking water of Dnipro, Ukraine) and in artificial seawater (3.5%NaCl solution, by mass, in distilled water) under conditions of cyclic daily changes in water temperature according to the graph in Fig. 1.

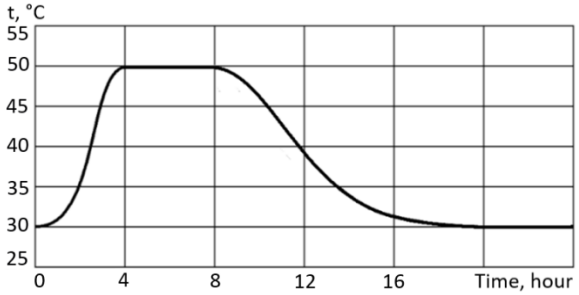

Figure 1. Daily change in water temperature in the climate chamber over time

The choice of accelerated studies on the corrosion resistance of bronzes under a daily cyclic temperature regime is since among the most challenging operating conditions for bronze parts is their use in marine diesel engines with a flowing overboard water-cooling system. The temperature of such water at the engine inlet should be within 35...45 °C and not exceed 50...55 °C at the outlet, which allows reducing the intensity of salt deposition in the engine breech space and the occurrence of silt in it. Seawater with a temperature even higher than 55 °C (up to 80 °C) is inherent for oil tank heating systems and heat exchangers. Such limits of changes in the temperature of fresh and seawater can also be observed in tropical and equatorial climatic zones.

As an indicator of the corrosion resistance of bronzes, the rate of their corrosion was determined by the decrease in the thickness of the sample during the year of its staying in an aggressive environment. For the calculation, data of a stable linear nature of the change in the thickness of the samples over time were used. That is, the change in the size of the samples from 21 (m_i) to 28 (m_j) per day of their staying in warm water and from 90 (m_i) to 180 (m_j) per day of their staying in cold water, mm/year:

$$W=365 \cdot (m_i\text{-}m_j)/[(\tau_j\text{-}\tau_i) \cdot S \cdot \rho], \quad (7)$$

where m_i, m_j – sample mass on the i-th and j-th day of the tests, g; τ_i, τ_j – i-th and j-th day of the tests; S – sample surface area, cm^2; ρ – sample density, g/cm^3.

Measurement of sample sizes to calculate their surface area before the start of the tests was carried out using a caliper with an error of 0.01 mm. The mass of the samples was measured on an analytical balance with an accuracy of 0.0001 g. The density of the samples was calculated based on the results of hydrostatic weighing in tap water at a temperature of 20 °C using the formula:

$$\rho = m_O \times \rho_{H_2O} / (m_O - m_{H_2O}), \quad (8)$$

where: m_O, m_{H_2O} – mass of the sample in air and water, respectively, g; ρ_{H_2O} - water density when weighed, g/cm³

Testing of "washer" type samples in warm standing water was carried out according to an accelerated scheme in the C&W Salt Spray Corrosion Test Cabinets mod. Cw1001. The layout of flat bronze samples (washers) for accelerated tests for non-contact corrosion in water is shown in Fig. 2.

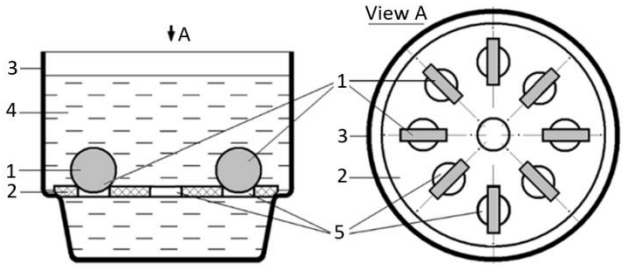

Figure 2. Layout of flat bronze samples (washers) in a container for accelerated testing of non-contact corrosion in standing warm water: 1 – flat sample (washer); 2 – porcelain stand; 3 – glass container; 4 – water; 5 – holes in the stand

The mass of the studied samples was measured every 7 days. Before weighing, the surface of the samples was cleaned of residues of corrosion products with a plastic brush and ultrasound. The cleaned samples were washed in flowing water and then dried at 105…110 °C for 1 hour and weighed. Upon completion of structural tests, the surface relief profile of the "washer" type samples from "as-cast" and heat-treated bronze BrA7K2O1.5Mts0.3 and their trace elements were studied. For these samples, a segment was cut out according to the scheme in Fig. 3a and after polishing and chemical etching with the chemical solution "Nital 2%" on area 4 (see Fig. 3b), using a Neophot 21 microscope at a magnification of ×400, the microstructure and surface relief profile of the samples were studied.

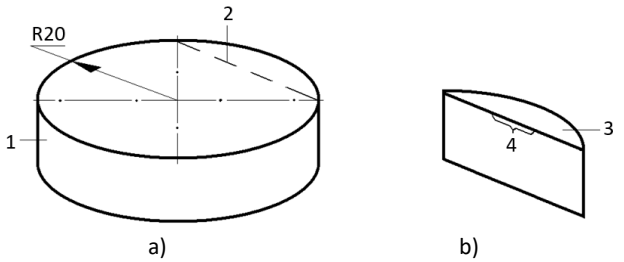

Figure 3. Sample cutting scheme (a) and the area of study of the relief profile of its surface (b): 1 – sample "washer"; 2 – sample cutting line; 3 – part of the washer for microstructural studies; 4 – area of study of the relief profile of the sample

The overall corrosion resistance in cold standing artificial seawater was carried out on cylindrical samples of not thermally treated ("as-cast") bronzes BrA11Zh6N6, BrA10Zh4N4, BrA10Mts2, BrA7K2O1.5Mts0.3 (K_R=0.33), BrA7K2O1.5Mts0.3 (K_R=0.48), BrA7K2O1.5Mts0.3 (K_R=0.52), BrA7K2O1.5Mts0.3 (K_R=0.61); BrA7K2O1.5Mts0.3 (K_R=0.76) and thermally treated bronze BrA7K2O1.5Mts0.3 (K_R=0.76).

For cylindrical samples of bronze BrA7K2O1.5Mts0.3, heat treatment was carried out before cutting them from cast blanks according to the following modes:

– heating the samples to 770 °C and holding for 30 min, quenching from 770 °C in water with a temperature of 20 °C;

– heating the samples to 770 °C and holding for 30 min, quenching from 770 °C in water with a temperature of 20 °C and ageing at 300 °C for 1 hour.

The layout of cylindrical bronze samples in a glass container during non-contact corrosion tests in standing artificial seawater at -1…+10 °C is presented in Fig. 4.

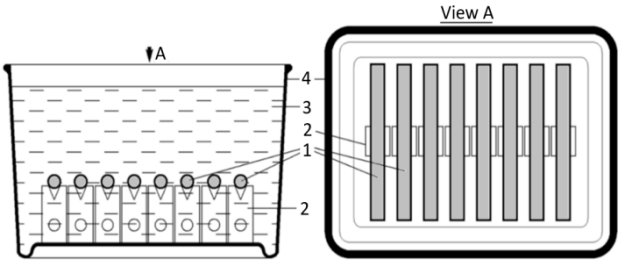

Figure 4. Arrangement of cylindrical bronze samples in a glass container during long-term tests for non-contact corrosion in standing artificial seawater at -1…+10 °C: 1 – samples; 2 – plastic support; 3 – seawater; 4 – glass container

Non-contact corrosion tests in standing cold seawater were carried out for 180 days in a refrigeration chamber at a temperature from -1 °C to +10 °C, which is characteristic of water in polar and temperate climatic zones. The mass of the samples was measured every 10 days with preparation for weighing using the "washer" sample method. The studies used cylindrical samples with dimensions ∅16×140 mm, which were cut from cast blanks ∅20×150 mm, which were cast in a sand-sodium-silicate (sand) casting mold, and blanks 20×20×150 mm, which were cast in not covered with refractory paint steel chill mold with an initial temperature of 140…150 °C.

Of the above-mentioned bronze grades, bronze grades BrA11Zh6N6, BrA10Zh4N4, BrA10Mts2, and BrO6Ts6S3 were used for comparison.

4 RESULTS AND DISCUSSION

General corrosion resistance of bronzes in standing warm tap water. According to the results of visual observation of the corrosion process, it was found that during the tests, single gas bubbles up to 0.5 mm in size periodically appeared on the surfaces of the samples, and a layer of white gelatinous substance appeared on and under the samples. At the same time, the initial colour and shine of the samples after their exposure for 28 days in standing warm tap water with a cyclic change in its temperature from 30 to 50 °C practically did not change, as evidenced by the appearance of the samples in Fig. 5, where heat treatment by quenching and ageing is designated as Q+A.

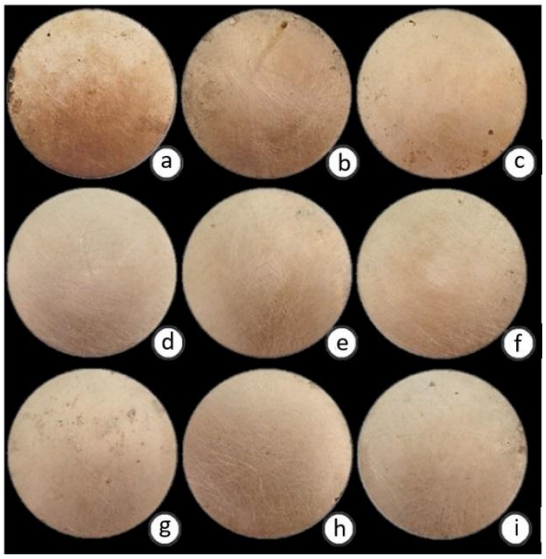

Figure 5. Appearance of bronze samples BrA10Zh4N4 (a), BrA9Zh3L (b), BrO6Ts6S3 (c), BrA7K2O1.5Mts0.3 (K_R=0.34) (d), BrA7K2O1.5Mts0.3 (K_R=0.57) (e), BrA7K2O1.5Mts0.3 (K_R=0.77) (f), BrA7K2O1.5Mts0.3 (K_R=0.34, Q+A) (g), BrA7K2O1.5Mts0.3 (K_R=0.57, G+S) (h), BrA7K2O1.5Mts0.3 (K_R=0.77, G+S) (i) after their exposure in standing warm tap water with cyclic temperature changes

The dependences of the change in the mass of the studied bronze samples over time, which were in such conditions for 28 days, are presented in Fig. 6.

From the analysis of the dependences in Fig. 6 it follows that, with the exception of the BrO6C6C3 bronze, all other studied bronzes are characterized by almost absolute stability in standing warm tap water, i.e., these bronzes have 1 point of stability. At the same time, the corrosion rate of samples from the BrO6C6C3 bronze was 0.0017±0.0001 mm/year, which corresponds to the second point of corrosion resistance.

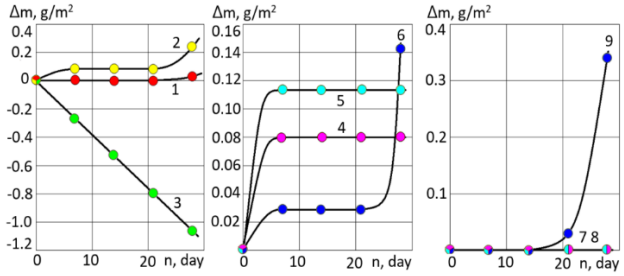

Figure 6. Change in mass of bronzes over time, which were in standing warm tap water with daily cyclic water change from 30 to 50 °C: 1 – BrA10Zh4N4; 2 – BrA9Zh3L; 3 – BrO6Ts6S3; 4 – BrA7K2O1.5Mts0.3 (K_R=0.34); 5 – BrA7K2O1.5Mts0.3 (K_R=0.57); 6 – BrA7K2O1.5Mts0.3 (K_R=0.77); 7 – BrA7K2O1.5Mts0.3 (K_R=0.34, Q+A); 8 – BrA7K2O1.5Mts0.3 (K_R=0.57, Q+A); 9 – BrA7K2O1.5Мц0.3 (KR=0.77, Q+A)

From the point of view of the kinetics of the general corrosion of the studied samples, the following features of the process should be noted:

– the process of changing the mass of samples of the BrO6C6C3, BrA9Zh3L bronzes and "as-cast" samples of the BrA7K2O1.5Mts0.3 bronze, regardless of the value of their K_R criterion, practically begins immediately after their immersion in fresh water, i.e., without an incubation period;

– the process of changing the mass of BrA10Zh4N4 bronze samples and heat-treated BrA7K2O1.5Mts0.3 bronze samples, regardless of the value of their K_R criterion, begins after a certain incubation period, which, according to the dependencies in Fig. 6, is about 21 days for BrA10Zh4N4 bronze samples, 14 days for heat-treated BrA7K2O1.5Mts0.3 bronze samples with K_R = 0.77 and more than 28 days for heat-treated BrA7K2O1.5Mts0.3 bronze samples with K_R = 0.34 and K_R = 0.57;

– for "as-cast" samples of bronze BrA7K2O1.5Mts0.3 with K_R = 0.34 and K_R = 0.57, the increase in mass is observed only during the first 7 days of testing and subsequently (up to the 28th day of testing) their mass does not change;

– the mass of bronze BrA10Zh4N4, BrA9Zh3L samples, and samples of "as-cast" and heat-treated bronze BrA7K2O1.5Mts0.3 remains unchanged until the 21st day of testing, after which their mass increases;

– among the studied bronzes, according to the adopted research methodology, the highest relative corrosion resistance is possessed by heat-treated bronze samples BrA7K2O1.5Mts0.3 with the values of the criterion K_R = 0.34 and K_R = 0.57.

The presence of an incubation period in the studied samples is probably explained by the presence of a relatively thick layer of a protective Al_2O_3 film on their surfaces in the initial state. The cyclical change in the rate of increase in the mass of samples from bronzes BrA10Zh4N4, BrA9Zh3L, and samples of "raw" and heat-treated bronze BrA7K2O1.5Mts0.3 with K_R=0.77 is probably due to the insufficient strength of the protective layer on their surfaces, which, with a cyclic change in temperature under conditions of cyclic increase and decrease in the size of the samples, leads to its destruction. The appearance of gas bubbles and a white precipitate during the tests of the samples is apparently explained by the appearance of a protective Al_2O_3 layer on the surfaces of the samples by sequentially passing the following chemical reactions:

$$2Al + 6H_2O \rightarrow 2Al(OH)_3 + 3H_2\uparrow, \quad (9)$$

$$4Al + 3O_2 \rightarrow 2Al_2O_3, \quad (10)$$

According to this the gas bubbles on the samples are hydrogen, and the sediment under the samples (a white, gelatinous substance that is poorly soluble in water) is aluminum hydroxide, which is limitedly soluble in water.

General corrosion resistance of bronzes in standing warm artificial seawater. According to the results of visual observation, it was found that during the tests, single gas bubbles up to 0.5 mm in size appeared on the surfaces of the bronze samples. A layer of grey-blue or brown sediment appeared under the samples, and the surfaces of the samples acquired a color from reddish-brown to black or several colors. The appearance of the samples of the studied bronzes after their exposure for 28 days in seawater with a cyclic change in its temperature from 30 to 50 °C is presented in Fig. 7. The dependence of the change in the mass of the studied bronze samples over time, which were in such conditions for 28 days, is presented in Fig. 8.

The histogram of the rate of overall corrosion resistance of bronzes in artificial seawater with a daily cyclic temperature change from 30 to 50 °C is presented in Fig. 9.

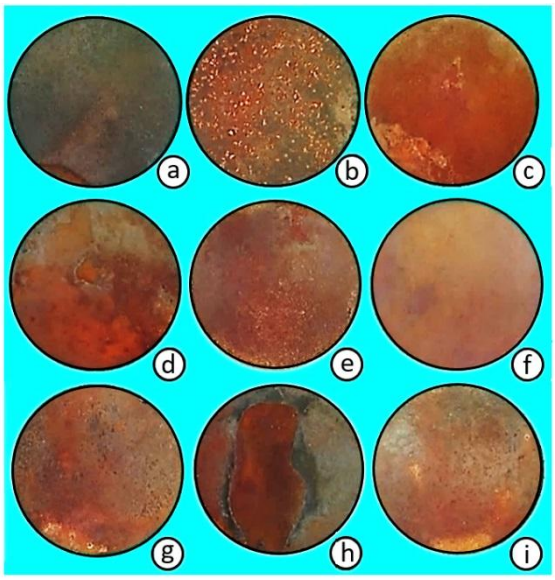

Figure 7. Appearance of bronze samples BrA10Zh4N4 (a), BrA9Zh3L (b), BrO6Ts6S3 (c), BrA7K2O1.5Mts0.3 (K_R=0.34) (g), BrA7K2O1.5Mts0.3 (K_R=0.57) (d), BrA7K2O1.5Mts0.3 (K_R=0.77) (e), BrA7K2O1.5Mts0.3 (K_R=0.34, Q+A) (g), BrA7K2O1.5Mts0.3 (K_R=0.57, Q+A) (h), BrA7K2O1.5Mts0.3 (K_R=0.77, Q+A) (i) after their exposure in standing warm artificial seawater with cyclic temperature changes

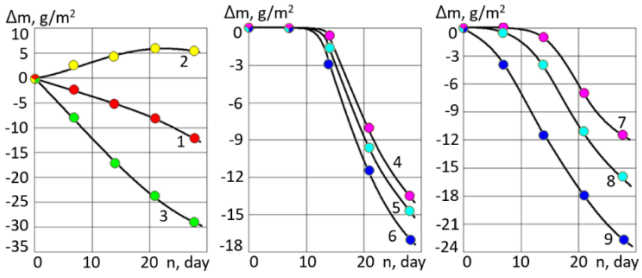

Figure 8. Change in mass of bronzes over time, which were in standing artificial warm sea water with daily cyclic temperature changes: 1 – BrA10Zh4N4; 2 – BrA9Zh3L; 3 – BrO6Ts6S3; 4 – BrA7K2O1.5Mts0.3 (K_R=0.34); 5 – BrA7K2O1.5Mts0.3 (K_R=0.57); 6 – BrA7K2O1.5Mts0.3 (K_R=0.77); 7 – BrA7K2O1.5Mts0.3 (K_R=0.34, Q+A); 8 – BrA7K2O1.5Mts0.3 (K_R=0.57, Q+A); 9 – BrA7K2O1.5Мц0.3 (K_R=0.77, Q+A)

Based on the nature of the location of corrosion products on the surfaces of samples made of BrA10Zh4N4 bronze and heat-treated BrA7K2O1.5Mts0.3 bronze with K_R=0.57 (see Fig. 7a,h), their corrosion is continuous, and the corrosion products arise according to reactions (1)…(5) and, accordingly, are arranged in layers, since a black layer of copper oxide (CuO) is located above the red-brown layer (Cu_2O). In this case, the adhesion strength between these layers is so low that the copper oxide layer is removed even by slowly rising flows of seawater that arise when its temperature changes.

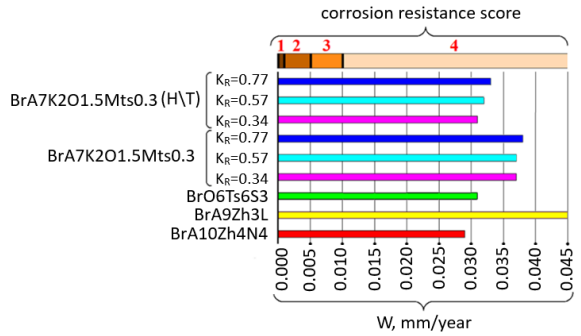

Figure 9. Histogram of the rate of general corrosion resistance of bronzes in standing artificial seawater with a daily cyclic change in temperature in the range from 30 to 50 °C (H\T – samples after quenching and aging)

The surface of all other bronzes, except for BrA9Zh3L bronze, is covered with a continuous layer of red-brown colour, which, according to reactions (1)…(5), represents Cu_2O and occurs on the surface of the Al_2O_3 layer, which is in direct contact with the surfaces of the samples.

As for the BrA9Zh3L bronze samples, on their surfaces, together with Cu and Al, its iron-containing phase reacts with the components of seawater according to chemical reactions (1)…(5) to form $Fe(OH)_2$, which is oxidized by oxygen dissolved in seawater to $Fe(OH)_3$. At the same time, the formed $Fe(OH)_3$ remains on the surface of the bronze in the form of local growths, which increases the mass of the samples over time and is a witness to the passage of pitting corrosion.

Since the iron-containing phase in the structure of bronze has a localized nature of location, at a certain time of the tests, such a phase in the surface layer of the samples disappears, but at the same time, the corrosion process continues according to reactions (1)…(5) and the mass of the bronze samples begins to decrease. That is, for the above reasons, a dense passivating film is not formed on the surface of the BaA9Zh3L bronze samples, and with an increase in the number and size of ulcers on the surface of the samples, the areas of their contact with seawater also increase, which also contributes to an increase in the rate of their corrosion. As a result, among the studied bronze grades (see Fig. 9), samples made of BrA9Zh3L bronze have the lowest corrosion resistance.

From the point of view of the kinetics of the general corrosion of the studied samples, the following should be noted:

– according to the course of the dependences in Fig. 8, only "as-cast" bronzes BrA7K2O1.5Mts0.3 (regardless of the value of the K_R criterion) in standing warm artificial seawater in the kinetics of the general corrosion have an incubation period of at least 7 days;

– the corrosion resistance in standing warm artificial seawater of "as-cast" bronze BrA7K2O1.5Mts0.3 is lower than that of the heat-treated one and does not depend much on the value of the K_R criterion, although it increases somewhat with a decrease in K_R, which follows from the analysis of the histogram in Fig. 10;

– a decrease in the fluidity of the corrosion due to longer hours of testing, probably, due to the increased thickness and density of the protective layer on the surface of the bronze, as well as outgoing micro-roughness of the surfaces of the specimens, not taking into account the selective interaction in local areas of specific structural components of studied bronzes, which follows from analysis of the image's comparison in Fig. 11;

– from the analysis of the comparison of the appearance of the relief profiles and microstructures of the BrA7K2O1.5Mts0.3 bronze samples in Fig. 12, it follows that its corrosion resistance under the accepted test conditions, in contrast to the statements of R. Ferrara and T. Caton (1982) and M. Fuller et al. (2007), does not depend on the sizes of its structural components.

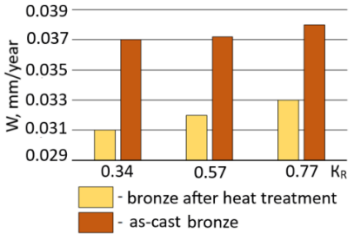

Figure 10. Corrosion rates in standing warm artificial seawater of "as-cast" and heat-treated bronze BrA7K2O1.5Mts0.3 depending on the value of the criterion K_R

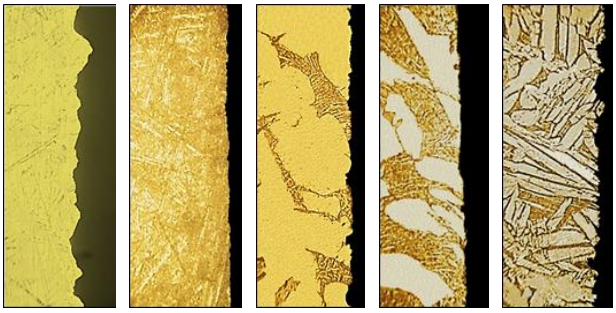

Figure 11. Appearance of the surface profile of bronze samples BrA7K2O1.5Mts0.3 before the beginning (a) and after the end (b, c, d, e) of corrosion resistance tests (×400)

The uniformity of the distribution of corrosion marks on the flat surfaces of the studied samples of BrA7K2O1.5Mts0.3 bronze, which was assessed based on the results of visual inspection of the samples, indicates that in all cases the corrosion is continuous in nature, and in the castings from which the "washer" type samples were cut, no external signs of macro-liquation processes that could occur during the solidification of the original castings.

General corrosion resistance of bronzes in standing cold artificial seawater. According to the results of visual observation of the corrosion process, it was found that during the tests the surfaces of some samples began to darken and changed their original golden hue to dark red or brown-black, which is evidenced, in particular, by the appearance of the samples in Fig. 12.

Figure 12. Appearance of the machined surfaces of "as-cast" bronze samples cast in a sand mold, after their exposure to standing seawater for 180 days

At the same time, a layer of white, gray or greenish-blue gelatinous substance appeared on the samples, which, as it accumulated, flowed from the surfaces of the samples.

The dependences of the change in temperature and mass of the studied bronze samples over time, which were in cold, standing artificial seawater for 180 days, are presented in Fig. 13.

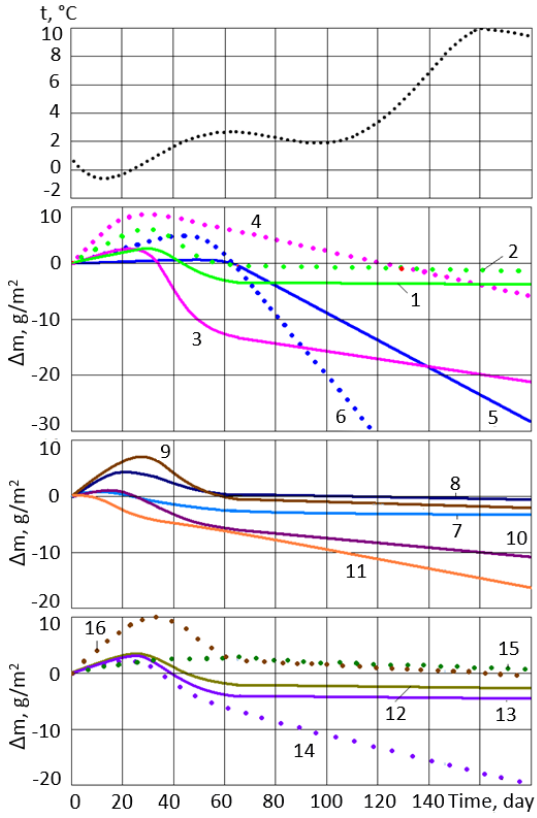

Figure 13. Dependences of changes in temperature (t) of seawater and mass (Δm) over time of bronze samples:

1 – BrA11Zh6N6 (c); 2 – BrA11Zh6N6 (s); 3 – BrA10Zh4N4 (c); 4 – BrA10Zh4N4 (s); 5 – BrA10Mts2 (c); 6 – BrA10Mts2 (s); 7 – BrA7K2O1.5Mts0.3(c, K_R=0.33); 8 – BrA7K2O1.5Mts0.3 (c, K_R=0.48); 9 – BrA7K2O1.5Mts0.3 (c, K_R=0.52); 10 – BrA7K2O1.5Mts0.3 (c, K_R=0.61); 11 – BrA7K2O1.5Mts0.3 (c, K_R=0.76); 12 – BrA7K2O1.5Mts0.3 (c, K_R=0.76, Q); 13 – BrA7K2O1.5Mts0.3 (c, K_R=0.76, Q+A); 14 – BrA7K2O1.5Mts0.3 (s, K_R=0.76); 15 – BrA7K2O1.5Mts0.3 (s, K_R=0.76, Q); 16 – BrA7K2O1.5Mts0.3 (s, K_R=0.76, Q+A), (s) – bronze cast in a sand mold; (c) – bronze cast in a chill mold; Q – bronze after quenching; Q+A – bronze after quenching followed by aging

Compared with the data on the corrosion rate in warm, standing artificial seawater, the corrosion rate in cold, standing artificial seawater is significantly lower, which is explained not only by the water temperature, but also by the character of the change in its temperature during the tests.

The results of mathematical processing of the data in Fig. 13 are presented in Fig. 14 and Fig. 15.

From the analysis of the dependences in Fig. 13, it follows that from the moment of immersion of the samples in cold standing artificial seawater, their mass begins to grow, which is probably due to an increase in the thickness of the protective film of Al_2O_3 by chemical reactions (1)…(5), (9), (10). That is, along with the appearance of Al_2O_3, aluminum hydroxide also appears. This is a gelatinous substance of white color, according to the results of visual observation.

Most likely that simultaneously with the appearance of aluminum oxide and hydroxide, chlorides and oxides of less chemically active bronze components, in particular, copper, appear on the surface of the samples. The resulting chemical compounds of other chemical elements not only give aluminum hydroxide a certain color, which was established by the results of visual observation. But also, apparently, when a certain critical amount is reached, they begin to constantly violate the density of the existing Al_2O_3 layer. As a result, over time, the growth of the mass of the studied bronze samples stops, after which it begins to decrease, and after a certain time, the mass of the samples becomes less than the initial one. Perhaps, such a change in the mass of the samples is due to the fact that the rate of the chemical process according to reaction (4) exceeds the rate of the chemical process according to reaction (5). In this regard, it is also appropriate to noting the bronze BrA7K2O1.5Mts0.3 with KR=0.76, which was cast in a sand mold and quenched (see dependence 15 in Fig. 13), in which the mass also decreased during the research (for 180 days) but did not become less than the initial one.

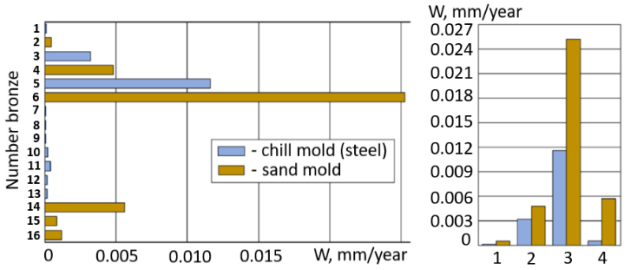

Figure 14. Rate of unbound corrosion of bronzes in standing artificial seawater with a temperature of -1…+10 °C (a): 1 – BrA11Zh6N6 (c); 2 – BrA11Zh6N6 (s); 3 – BrA10Zh4N4 (c); 4 – BrA10Zh4N4 (s); 5 – BrA10Mts2 (c); 6 – BrA10Mts2 (s); 7 – BrA7K2O1.5Mts0.3 (c, K_R=0.33); 8 – BrA7K2O1.5Mts0.3 (c, K_R=0.48); 9 – BrA7K2O1.5Mts0.3 (c, K_R=0.52); 10 – BrA7K2O1.5Mts0.3 (c, K_R=0.61); 11 – BrA7K2O1.5Mts0.3 (c, K_R=0.76); 12 – BrA7K2O1.5Mts0.3 (c, K_R=0.76, Q); 13 – BrA7K2O1.5Mцb0.3 (c, K_R=0.76, Q+A); 14 – BrA7K2O1.5Mts0.3 (s, K_R=0.76); 15 – BrA7K2O1.5Mts0.3 (s, K_R=0.76, Q); 16 – BrA7K2O1.5Mts0.3 (s, K_R=0.76, Q+A) (a) and bronzes cast in a chill and sand mold (b): 1 – BrA11Zh6N6; 2 – BrA10Zh4N4; 3 - BrA10Mts2; 4 – BrA7K2O1.5Mts0.3 (K_R=0.76); (c) – bronze cast in chill mold; (s) – bronze cast in sand mold; Q – bronze after quenching; Q+A – bronze after quenching followed by aging

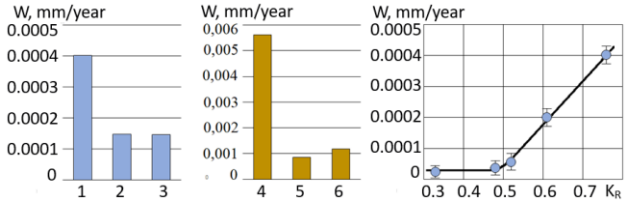

Figure 15. Rate of unbound corrosion in standing artificial seawater with a temperature of -1…+10 °C bronze (a): 1 – BrA7K2O1.5Mts0.3 (c, K_R=0.76); 2 – BrA7K2O1.5Mts0.3 (c, K_R=0.76, Q); 3 – BrA7K2O1.5Mts0.3 (c, K_R=0.76, Q+A); 4 – BrA7K2O1.5Mts0.3 (s, K_R=0.76); 5 – BrA7K2O1.5Mts0.3 (s, K_R=0.76, Q); 6 – BrA7K2O1.5Mts0.3 (s, K_R=0.76, Q+A) and "as-cast" bronze BrA7K2O1.5Mts0.3, which was cast in a chill mold (b), from the value of the criterion K_R; (c) – bronze cast in chill mold; (s) – bronze cast in sand mold; Q – bronze after quenching; Q+A – bronze after quenching followed by aging

During this period of research, samples of all the studied bronzes lose mass, as a rule, according to a linear law, but with different intensity, which is explained by the difference between the samples in chemical and phase composition, and the conditions of their preparation for the tests.

From the analysis of the histogram in Fig. 15, a it follows that the corrosion resistance of bronze BrA7K2O1.5Mts0.3 in terms of the corrosion rate in standing artificial seawater with a temperature of -1…+10 °C is comparable, and in some cases even exceeds its indicators inherent in marine aluminum-nickel (NAB) and aluminum-manganese (MAB) bronzes.

From the analysis of the dependences of the rate of general corrosion of bronze BrA7K2O1.5Mts0.3 in standing artificial seawater with a temperature of -1…+10 °C (see Fig. 15) it follows that under these conditions, heat treatment of bronzes significantly (by several times) increases their corrosion resistance regardless of the mold in which the sample blank was cast. In this case:

– both quenching and quenching followed by aging of bronze increase their corrosion resistance, practically, to the same level (see Fig. 14a and Fig. 15a);

– the corrosion rate of samples from blanks that were cast in a chill mold is an order of magnitude lower than that of samples from blanks that were cast in a sand mold and, in fact, for samples from blanks that were cast in a sand mold, the effect of heat treatment on the corrosion resistance of bronze BrA7K2O1.5Mts0.3 in cold standing artificial seawater is similar to that in warm standing artificial seawater (see Fig. 14, a and Fig. 15, a);

– on a ten-point scale for evaluating corrosion resistance in cold, standing artificial seawater, only "as-cast" bronze BrA7K2O1.5Mts0.3, the workpiece of which was cast in a sand mold, has a corrosion resistance score of 2, while all heat-treated bronzes and "as-cast" bronze BrA7K2O1.5Mts0.3, the workpiece of which was cast in a chill mold, have a corrosion resistance score of 1.

Table 4. Corrosion resistance score of bronze BrA7K2O1.5Mts0.3 on a ten-point scale

Foundry mold	Heat treatment (Q –quenching, A – ageing)			Corrosion resistance score of bronze BrA7K2O1.5Mts0.3 at K_R					
	no	Q	Q+A	0.33-0.34	0.48	0.52	0.57	0.61	0.76-0.77
warm, standing tap water with a cyclical nature of temperature changes									
sandy	+			1			1		1
sandy			+	1			1		1
warm, standing artificial seawater with cyclical temperature changes									
sandy	+			4			4		4
sandy			+	4			4		4
cold, standing artificial seawater with uncontrolled temperature changes									
sandy	+								3
sandy		+							2
sandy			+						2
chill mold	+			1	1	1		1	1
chill mold		+							1
chill mold			+						1

Unlike the "as-cast" samples, which were made from blanks cast in a sand mold and tested in warm, standing artificial seawater, the "as-cast" samples cast in a chill mold and tested in cold, standing artificial seawater have a dependence between their corrosion rate and the value of the K_R criterion, as evidenced by the dependence in Fig. 15, b. From the analysis of the dependence in Fig. 15, b, it follows that the corrosion rate of "as-cast" bronze BrA7K2O1.5Mts0.3 in cold, standing artificial seawater is practically independent of the value of its K_R criterion in the range of its changes from 0.33 to 0.47 and increases linearly by an order of magnitude with an increase in K_R to 0.77. It is obvious that the established regularities for BrA7K2O1.5Mts0.3 bronze are associated with the microstructural non-identity of the samples from the point of view of phase composition, which is due to changes in the chemical composition of the bronzes, the conditions of their solidification and heat treatment.

Generalized data on the corrosion resistance of bronze BrA7K2O1.5Mts0.3 on a ten-point scale are given in Table 4.

From the analysis of the data in Table 4, it follows that in different environments and test conditions, bronze BrA7K2O1.5Mts0.3 is characterized by a different level of corrosion resistance. In general, according to the test results, bronze BrA7K2O1.5Mts0.3, regardless of the value of its K_R indicator, can be considered a very corrosion-resistant alloy in both tap water and artificial seawater. At the same time, the level of corrosion resistance of bronze BrA7K2O1.5Mts0.3 is practically the same as the similar indicator of bronzes for marine use, BrA11Zh6N6 and BrA10Zh4N4.

5 CONCLUSIONS

Except for BrO6C6S3 bronze, all other bronzes studied in this work are absolutely stable in warm standing tap water with a cyclic change in temperature from 30 to 50 °C.

The longest incubation period in warm standing tap water for BrA10Zh4N4 bronze reaches 21 days, and in heat-treated (quenching + aging) BrA7K2O1.5Mts0.3 bronzes with K_R = 0.34 and K_R = 0.57 it exceeds 28 days.

With the exception of BrA9Zh3L bronze, all other bronzes studied in this work are stable in warm standing artificial seawater with a daily change in temperature from 30 to 50 °C and have a 4th corrosion resistance score on a ten-point scale.

In warm, standing artificial seawater with a daily temperature change of 30 to 50 °C, BrA7K2O1.5Mts0.3 bronze after heat treatment is characterized by greater corrosion resistance (lower corrosion rate) than without heat treatment. At the same time, without heat treatment, the greatest corrosion resistance is possessed by BrA7K2O1.5Mts0.3 bronzes with a value of K_R = 0.37…0.63, and among the heat-treated bronzes - with a value of K_R = 0.47…0.74. That is, it is permissible to assume that the greatest corrosion resistance is possessed by BrA7K2O1.5Mts0.3 bronze with a value of K_R = 0.47…0.63.

Corrosion in BrA7K2O1.5Mts0.3 bronze samples, both before and after heat treatment, is continuous. At the same time, both in warm and cold standing artificial seawater, heat treatment increases the corrosion resistance of BrA7K2O1.5Mts0.3 bronze samples. "As-cast" and heat-treated BrA7K2O1.5Mts0.3 bronze in cold standing artificial seawater is more resistant to corrosion if it is cast in a chill mold (the corrosion rate of bronze that was cast in a chill mold is an order of magnitude lower than the corrosion rate of bronze that was cast in a sand mold).

In all corrosive environments used in the work, among other factors, its heat treatment is more dominant from the point of view of the corrosion resistance of BrA7K2O1.5Mts0.3 bronze.

Since the level of corrosion resistance of cast structural bronze BrA7K2O1.5Mts0.3 is practically the same as the similar indicator of marine bronzes BrA11Zh6N6 and BrA10Zh4N4. This is the reason to recommend it for use in industry as a non-magnetic substitute for known magnetic marine bronzes.

ACKNOWLEDGMENTS

The authors would like to thank the KEGA grant agency for supporting research work and co-financing the project KEGA 008TUKE-4/2025.

REFERENCES

[Aliyu 2025] Aliyu, A., Bishop, D.P., Nasiri, A. Effect of heat treatment on microstructural evolution and

corrosion behavior of wire-arc additive manufactured nickel aluminum bronze alloy. Corrosion Science, 2025, Vol. 249, pp. 1-16.

[Asgari 2021] Asgari, M., Foratirad, H., Golabadi, M., Kar M. Investigation of the corrosion behavior of aluminum bronze alloy in alkaline environment. Materialwissenschaft und Werkstofftechnik, 2021, Vol. 52, No. 5, pp. 511-519.

[Cargua 2021] Cargua, V., Vasconez-Nunez, D.C., Tello-Oquendo, F.M. Analysis of the Corrosion Resistance of Bronze to Aluminium (ASTM B 824) in a Corrosive Environment Controlled with an Artificial Seawater Solution. Ecuadorian Journal of Steam, 2021, Vol. 1, No. 1.

[Coranic 2023] Coranic, T. and Mascenik, J. Experimental Measurement of Dynamic Characteristics of Structural Units. Processes, 2023, Vol. 11, No. 12, 3333. DOI: 10.3390/pr11123333

[Dyadyura 2017a] Dyadyura, K.O., Sukhodub, L.F. Magnesium-based matrix composites reinforced with nanoparticles for biomedical applications. In: Proc. of 2017 IEEE 7th Int. Conf. on Nanomaterials: Applications and Properties - NAP 2017, 2017, 04NB14.

[Dyadyura 2017b] Dyadyura, K., et al. Influence of roughness of the substrate on the structure and mechanical properties of TiAlN nanocoating condensed by DCMS. In: Proc. of 2017 IEEE 7th Int. Conf. on Nanomaterials: Applications and Properties - NAP 2017, 2017, 01FNC10.

[Gaspar 2018] Gaspar, S., Coranic, T., Pasko, J. Influence of Die Casting Factors and of Hardening Temperature Upon Mechanical Properties of a Die Cast. MM Science J., 2018, Vol. December, pp. 2639-2642. DOI: 10.17973/MMSJ.2018_12_2018108

[Harnicarova 2019] Harnicarova, M., et al. Study of the influence of the structural grain size on the mechanical properties of technical materials. Materialwissenschaft und Werkstofftechnik, 2019, Vol. 50, pp. 635-645. ISSN 0933-5137.

[Jurko 2011] Jurko, J., Panda, A., Behun, M. Prediction of a new form of the cutting tool according to achieve the desired surface quality. Applied Mechanics and Materials, 2013, Vol. 268, pp. 473-476.

[Jurko 2012] Jurko, J., Dzupon, M., Panda, A., Zajac, J. Study influence of plastic deformation a new extra low carbon stainless steels XCr17Ni7MoTiN under the surface finish when drilling. Advanced Materials Research, 2012, Vol. 538-541, pp. 1312-1315.

[Jurko 2013] Jurko, J., Panda, A., Behun, M. Prediction of a new form of the cutting tool according to achieve the desired surface quality. Applied Mechanics and Materials, 2013, Vol. 268, No. 1, pp. 473-476.

[Kimstach 2025a] Kimstach, T.V., Uzlov, K.I. Alloying elements synergic and selective effect on mechanical properties of Cu-Al-Si-Sn-Mn system bronze. Modern Problems of Metalurgy, 2025, Vol. 28, pp. 162-183.

[Kimstach 2025b] Kimstach, T.V., et al. Assessing criteria for casting and deformation suitability of metals and alloys. Naukovyi Visnyk Natsionalnoho Hirnychoho Universytetu, 2025, Vol. 1, pp. 40-47.

[Krenicky 2024] Krenicky, T., Goncharov, O.Y., Kuchar, J., et al. Chemical Vapor Deposition of Tantalum Carbide in the TaBr5–CCl4–Cd System. Coatings, 2024, Vol. 14, No. 5, 547. DOI: 10.3390/coatings14050547

[Kuric 2022] Kuric, I., et al. Approach to Automated Visual Inspection of Objects Based on Artificial Intelligence. Applied Sciences, 2022, Vol. 12, Issue 2. DOI: 10.3390/app12020864

[Li 2019] Li, Y., Lian, Y., Sun, Y.J. Cavitation erosion behavior of friction stir processed nickel aluminum bronze. Journal of Alloys and Compounds, 2019, Vol. 795, pp. 233-240.

[Li 2022] Li, Z.X., Zhang, L.M., Udoh, I., Ma, A.L., Zheng, Y.G. Deformation-induced martensite in 304 stainless steel during cavitation erosion: Effect on passive film stability and the interaction between cavitation erosion and corrosion. Tribology International, 2022, Vol. 167, 107422.

[Luo 2018] Luo, Q., et al. The synergistic effect of cavitation erosion and corrosion of nickel-aluminum copper surface layer on nickel-aluminum bronze alloy. Journal of Alloys and Compounds, 2018, Vol. 747, pp. 861-868.

[Mascenik 2024] Mascenik, J., Coranic, T., Kuchar, J., Hazdra, Z. Influence of Selected Parameters of Zinc Electroplating on Surface Quality and Layer Thickness. Coatings, 2024, Vol. 14, No. 5, 579. https://doi.org/10.3390/coatings14050579

[Mayer 2022] Mayer, A.R., et al. Evaluation of cavitation/corrosion synergy of the Cr3C2-25NiCr coating deposited by HVOF process. Ultrasonics Sonochemistry, 2022, Vol. 69, 105271.

[Nadolski 2017] Nadolski, M. The Evaluation of Mechanical Properties of High-tin Bronzes. Archives of Foundry Engineering, 2017, Vol. 17, No. 1, pp. 127-130.

[Nahornyi 2022] Nahornyi, V., et al. Method of Using the Correlation between the Surface Roughness of Metallic Materials and the Sound Generated during the Controlled Machining Process. Materials, 2022, Vol. 15, 823.

[Ocejo 2022] Ocejo, I.C., Moraleda, M.V.B., Linhardt, P. Corrosion Behavior of Heat-Treated Nickel-Aluminum Bronze and Manganese-Aluminum Bronze in Natural Waters. Metals, 2022, Vol. 12, No. 3, 380. https://doi.org/10.3390/met12030380

[Panda 2011a] Panda, A., Duplak, J., Jurko, J., Behun, M. Comprehensive Identification of Sintered Carbide Durability in Machining Process of Bearings Steel 100CrMn6. Advanced Materials Research, 2011, Vol. 340, pp. 30-33.

[Panda 2011b] Panda, A., Duplak, J., Jurko, J. Analytical expression of T-vc dependence in standard ISO 3685 for cutting ceramic. Key Engineering Materials, 2011, Vol. 480-481, pp. 317-322.

[Panda 2013a] Panda, A., Duplak, J., Jurko, J., Behun, M. New experimental expression of durability dependence for ceramic cutting tool. Applied Mechanics and Materials, 2013, Vol. 275-277, pp. 2230-2236.

[Panda 2013b] Panda, A., Duplak, J., Jurko, J., Pandova, I. Roller Bearings and Analytical Expression of Selected Cutting Tools Durability in Machining Process of Steel 80MoCrV4016. Applied Mechanics and Materials, 2013, Vol. 415, pp. 610-613.

[Qiao 2019] Qiao, L., Wu, Y.P., Hong, S., Cheng, J. Ultrasonic cavitation erosion mechanism and mathematical model of HVOF sprayed Fe-based amorphous/nanocrystalline coatings. Ultrasonics Sonochemistry, 2019, Vol. 52, pp. 142-149.

[Qin 2022] Qin, Z.B., et al. Effect of compressive stress on cavitation erosion-corrosion behavior of nickel-

aluminum bronze alloy. Ultrasonics Sonochemistry, 2022, Vol. 89, 106143.

[Siemek 2021] Siemek, K., et al. Defects studies of nickel aluminum bronze subjected to cavitation. Applied Surface Science, 2021, Vol. 546, 149107.

[Song 2015] Song, Q.N., Zheng, Y.G., Ni, D.R., Ma, Z.Y. Characterization of the Corrosion Product Films Formed on the As-Cast and Friction-Stir Processed Ni-Al Bronze in a 3.5 wt% NaCl Solution. Corrosion, 2015, Vol. 71, No. 5, pp. 606-614.

[Song 2022] Song, Q.N., Tong, Y., Li, H.L., Zhang, H.N., Xu, N. Corrosion and cavitation erosion resistance enhancement of cast Ni–Al bronze by laser surface melting. Journal of Iron and Steel Research International, 2022, Vol. 29, pp. 359-369.

[Song 2023] Song, Qi-n., Li, H.-l., Xu, N., Jiang Zh. Selective phase corrosion and cavitation erosion behaviors of various copper alloys in 3.5 % NaCl solutions with different pH values. Transactions of Nonferrous Metals Society of China, 2023, Vol. 33, No. 10, pp. 3039-3053.

[Tian 2022] Tian, Y., et al. Behavior of the hard phases of copper alloys subjected to cavitation erosion investigated by SEM observation. Tribology International, 2022, Vol. 174, 107771.

[Turtelli 2006] Turtelli, R.S, et al. Magnetic and structural characterization of as-cast and annealed melt- spun Fe80-xSi20Crx. Journal of Magnetism and Magnetic Materials, 2006, Vol. 304, No. 2, pp. E687-E689.

[Valicek 2016] Valicek, J., et al. Mechanism of Creating the Topography of an Abrasive Water Jet Cut Surface. Advanced Structured Materials, 2016, Vol. 61, pp. 111-120.

[Vinagre 2020] Vinagre, P.A., Simas, T., Cruz, E., Pinori, E., Svenson, J. Marine biofouling: a European database for the marine renewable energy sector. Journal of Marine Science and Engineering, Vol. 8, No. 7, 495. https://doi.org/10.3390/jmse8070495

[Wu 2015] Wu, Z., Cheng, Y.F., Liu, L., Lv, W., Hu, W. Effect of heat treatment on microstructure evolution and erosion-corrosion behavior of a nickel-aluminum bronze alloy in chloride solution. Corrosion Science, 2015, Vol. 98, pp. 260-270.

[Zaloga 2019] Zaloga, V., Dyadyura, K., Rybalka, I., Pandova, I. Implementation of Integrated Management System in Order to Enhance Equipment Efficiency. Management Systems inProduction Engineering, 2019, Vol. 4, pp. 221-226.

[Zaloga 2020] Zaloga, V., Dyadyura, K., Rybalka, I., Pandova, I., Zaborowski, T. Enhancing efficiency by implementation of integrated management system in order to align organizational culture and daily practice. Management Systems in Production Engineering, 2020, Vol. 28, No. 4, pp. 304-311.

[Zeng 2022] Zeng, S.Q., Hu, S.B., Cheng, G.K. Effect of shot peening on surface characterization and cavitation resistance of nickel aluminum bronze. Materials Today Communications, 2022, Vol. 33, 104767.

[Zhang 2019] Zhang, L.M., Ma, A.L., Yu, H., Umoh, A., Zheng, Y. Correlation of microstructure with cavitation erosion behaviour of a nickel-aluminum bronze in simulated seawater. Tribology International, 2019, Vol. 136, pp. 250-258.

CONTACTS:

Dr.h.c. Prof. Ing. Anton Panda, PhD.
Technical University of Kosice
Faculty of Manufacturing Technologies with a seat in Presov
Sturova 31, 080 001 Presov, Slovakia
e-mail: anton.panda@tuke.sk